plasma

MDPI

Article

A Global Model Study of Plasma Chemistry and Propulsion Parameters of a Gridded Ion Thruster Using Argon as Propellant

Bernardo Magaldi, Júlia Karnopp, Argemiro da Silva Sobrinho and Rodrigo Pessoa *

Laboratório de Plasmas e Processos, Instituto Tecnológico de Aeronáutica, São José dos Campos 12228-900, SP, Brazil; magaldi.ita@gmail.com (B.M.); julia_karnopp@outlook.com (J.K.); argemiro@ita.br (A.d.S.S.)
* Correspondence: rspessoa@ita.br; Tel.: +55-12-39475785

Abstract: This work reports on the (zero-dimensional) global model study of argon plasma chemistry for a cylindrical thruster based on inductively coupled plasma (ICP) whose output has a system of two grids polarized with each other with direct current potential. The global model developed is based on particle and energy balance equations, where the latter considers both charged and neutral species. Thus, the model allows the determination of the neutral gas temperature. Finally, this study also investigated the role of excited species in plasma chemistry especially in the ions production and its implications for propulsion parameters, such as thrust. For this, the study was carried out in two different scenarios: (1) one taking into account the metastable species Ar^r and Ar^p (multi-step ionization), and (2) the other without these species (single-step ionization). Results indicates a distinct behavior of electron temperature with radiofrequency (RF) power for the investigated cases. On the other hand, the gas temperature is almost the same for investigated power range of up to 900 W. Concern propulsion analysis, a thrust of 40 mN at 450 W was verified for case (1), which represents a remarkable thrust value for electric thrusters.

Keywords: argon plasma; inductively coupled plasma; global model; thruster; plasma parameters; propellant

Citation: Magaldi, B.; Karnopp, J.; da Silva Sobrinho, A.; Pessoa, R. A Global Model Study of Plasma Chemistry and Propulsion Parameters of a Gridded Ion Thruster Using Argon as Propellant. *Plasma* **2022**, *5*, 324–340. https://doi.org/10.3390/plasma5030025

Academic Editor: Andrey Starikovskiy

Received: 18 June 2022
Accepted: 26 July 2022
Published: 28 July 2022

1. Introduction

The global economic, social and environmental development face some problems and limitations due the necessity to improve information and communication technologies [1]. Efforts are currently being made to increase the capacity of fast and long-range telecommunications, added to the support of global information networks and the survey of natural resources and meteorological. It could be solved by space systems, such as the small constellations of nanosatellites in low orbits, close to Earth [2]. The interest in creating new space systems has grown in recent decades and the two of the biggest companies in the space industry, SpaceX and One Web, have announced their intentions to launch thousands of satellites in the next 5 years [2].

Satellites requires frequent correction and maintenance of the orbit. It implies an increase in propellant consumption and, consequently, the need for a small propulsion system with a high specific impulse [3]. One solution to this demand is electrical propulsion (EP) systems that accelerate ions to exhaust velocities one or two orders of magnitude greater than classical chemical motors, leading to improved specific impulse [4]. This feature dramatically reduces the amount of propellant needed, allowing for longer mission times and heavier payloads [4]. The downside is the low ion mass production rate, which is limited by the reduced electrical energy that can be made available on board, further limiting the thrust levels that can be achieved. EP systems are characterized by low thrusts and high specific impulses. These features are essential for orbital maneuvers, station

maintenance, flight formation, and end-of-life disposal of small constellation satellites intended for global internet coverage [4].

EP systems are classified according to the ion acceleration method, thus dividing it into three categories: electrothermal, electromagnetic, and electrostatic [5]. Each category has several different types of thrusters, with strengths and weaknesses, always requiring an assessment of which factors will be most important for the satellite or space probe mission. Among these categories, electrostatic thrusters are the ones that present several studies regarding the thruster and/or propellant [5–11].

In the gridded ion thruster (GIT), a type of electrostatic thruster, ions are accelerated by a stationary electric field. Ions are produced in a plasma (propellant) and extracted from it through electrically polarized grids with high velocities producing the thrust [5]. The plasma is usually generated in radio frequency inductively coupled plasma (RF-ICP) system [7]. Xenon gas is the most used propellant in the GIT due to its high molar mass and for being a noble gas with 131 atomic mass unit (amu) [8]. However, xenon is expensive and has an ionization threshold energy of 12.1 eV [12]. Another propellant that has been used in thrusters is argon gas [13–16]. It has low weight, 40 amu, and, consequently, highest exhaust velocities. However, it has a higher ionization threshold energy than xenon, i.e., 15.76 eV, which increases the energy consumption for ion production. However, the advantage of using argon is that it is cheaper than xenon.

In order to improve the efficiency of GIT and find the best propellant alternatives it is necessary to study gas ionization process. Computational modeling can efficiently contribute to such goals, saving time and resources. Plasma modeling allows the study of plasma chemistry and complements experimental diagnostics under test conditions that are experimentally inaccessible [17]. In plasma modeling, the global model stands out for allowing the studying of complex plasma chemistries with a low computational cost [18].

The global model is a zero-dimensional model originating from fluid theory [18]. It comprises a set of differential equations of species density and energy that are temporally solved. Some global models have been developed to study ion thruster systems. In 2012, Chabert et al. developed a global model for ICP-type ion thruster with grids to estimate the efficiency of the xenon propellant [19]. Chabert included the energy balance of the neutral species in global model and analyzed the effect of gas temperature in plasma chemistry. In 2016, Grondein et al. applied this model to iodine, thus taking a first comparison between the respective efficiencies of both propellants [12]. These models did not consider the external neutralizer, which was eventually included by Dietz et al. in 2020 [20]. To date, there is no global model in the literature for GIT using argon as propellant.

Argon plasma is composed of grounded state argon, Ar; argon ion, Ar^+; electrons, e^-; and several excited species. The excited species can be ionized and contribute to propulsion efficiency. For modeling argon plasma, some models consider only one excited specie, the metastable, Ar^m, and others also include the resonant, Ar^r, and 4p states, Ar^p. The metastable corresponds to states $^3P_0$ and $^3P_2$ and have a long lifetime compared to other excited species [21]. The states $^1P_1$ and $^3P_1$ compose the resonance level. The Ar^p is composed of the next ten energy levels in the range of 12.9–13.5 eV.

In this study, a global model for GIT was developed to analyze the argon plasma chemistry and investigate the gas ionization process. This work investigated the role of excited species in plasma chemistry, especially in ion production and its implications for propulsion parameters, such as thrust. Thus, this study was carried out in two different scenarios: (1) one taking into account the three excited species Ar^m, Ar^r, and Ar^p and the ionization of theme (multi-step ionization) and (2) the other without Ar^r and Ar^p species and considering only ionization from fundamental state (single-step ionization). The global model was developed taking as reference the models proposed by Chabert et al. [19] and Grondein et al. [12]. In the energy balance for neutral species, new terms were introduced to the equation to study the dependence of the gas temperature on collisional processes.

2. Global Model

In this global model, the thruster geometry consists of a cylindrical chamber of radius R and length L, so that the total internal area is $A = 2\pi R^2 + 2\pi RL$ and the volume is $V = \pi R^2 L$. At the propellant inlet, neutral gas is introduced at a fixed flow rate Q_0, while the opposite end features a pair of screen grid and accelerator grid, separated by a gap s, as shown in the scheme of Figure 1.

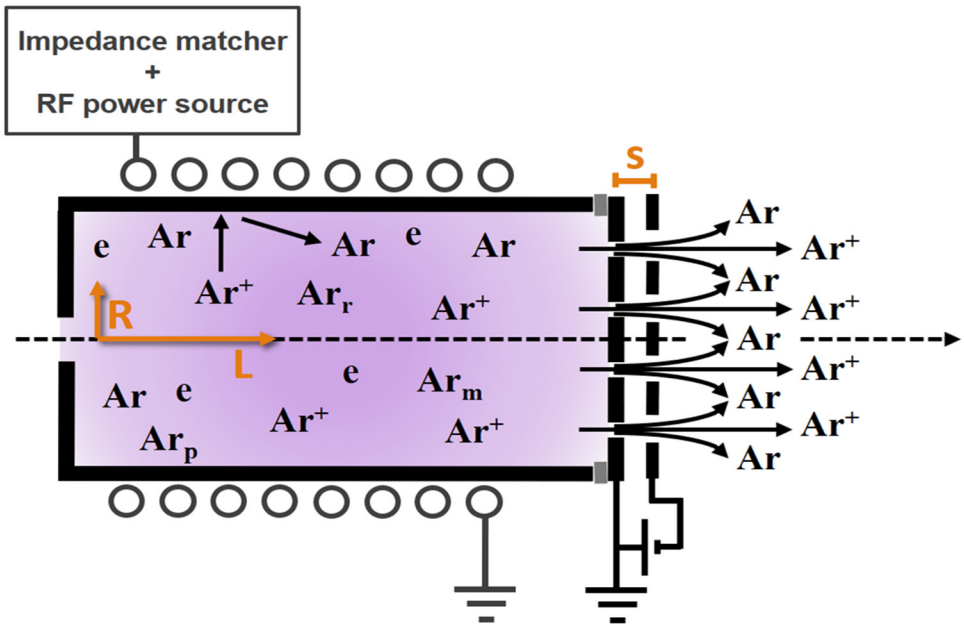

Figure 1. Schematic of the plasma thruster with grids, surrounded by a RF coil at 13.56 MHz. Argon gas is injected on the left and positive ions are accelerated by DC biased grids on the right.

Neutral gas flux is defined as $\Gamma_g = \frac{1}{4} n_g v_g$, where n_g is the neutral gas density and $v_g = \left(8k_B T_g / \pi M\right)^{0.5}$ is the average velocity of atoms as a function of gas temperature; T_g is expressed in Kelvin and M is the mass of the argon. The neutral gas flow out of the thruster through the area is given by $A_g = \beta_g \pi R^2$, where β_g is the transparency coefficient for neutral atoms. This can vary between $0 \leq \beta_g \leq 1$, and for $\beta_g = 0$ there is no neutral gas escape from the thruster. Analogously, the area through which the ions escape is $A_i = \beta_i \pi R^2$, denoting β_i as the grid transparency for ions, assuming that the ion transparency is independent of the ion mass.

Neutral flow out of the thruster depends on the gas density and gas temperature, when the thruster is turned on. Therefore, before the plasma is turned on, when it is in steady state, it is possible to determine the neutral gas flow rate as $Q_0 = \Gamma_{g0} A_g = \frac{1}{4} n_{g0} v_{g0} A_g$, where n_{g0} and v_{g0} are the neutral gas density and the mean velocity without plasma, respectively [22]. From the equation of state $p_0 = n_{g0} k_B T_{g0}$, by substituting the neutral gas density, we obtain:

$$p_0 = \frac{4 k_B T_{g0} Q_0}{v_{g0} A_g}. \tag{1}$$

The flow of ions leaving the impeller is composed of single ionized species, since the argon is at low pressure and its escape velocity is a function of the acceleration caused by the voltage difference between the two grids, V_{grid}, and elemental charge, e:

$$v_{beam} = \left(\frac{2eV_{grid}}{M}\right)^{0.5}, \tag{2}$$

Finally, by means of the volume averaging technique for a global model, a set of linear differential equations, which are composed of particle balance equations for each argon

gas/plasma species and two equations for the energy balance, is solved [23,24]. Details concerning these equations are presented in the next topics.

2.1. Particle Balance

In this model, a plasma was considered to be composed of three mutual particle interactions: between neutral atoms, positive ions with a single charge, and electrons. These interactions are listed in Table 1, which considers production and loss through many processes, including reactions between electrons and gas species, reactions between two gas species, the recombination of neutral species on the chamber walls, the neutralization of positive ions on the walls of the chamber, the quenching of the metastable states in the chamber walls, and the insertion of gas species into the chamber and pumping out of these species. For each species, there is a particle equilibrium equation given by [25]:

$$\frac{dn^{(X)}}{dt} = \sum_i R^{(X)}_{production,i} - \sum_i R^{(X)}_{loss,i}, \tag{3}$$

where $\sum_i R^{(X)}_{production,i}$ represents the sum of all reaction rates that contribute to the production of species X, and $\sum_i R^{(X)}_{loss,i}$ represents the sum of all reaction rates that contribute to the loss of species X. There is a reaction rate for each reaction considered in the model. Reaction rates are calculated as the product of the densities of the species participating in the reaction and the rate coefficient of this reaction. The electron density is obtained through charge neutrality [26]:

$$n_e = n^+, \tag{4}$$

where n_e is the electron density and n^+ is the ion density.

2.1.1. Neutralization of Positive Ions on Chamber Walls

Ions can diffuse to chamber walls and are neutralized when they collide with the wall surface. Their reaction constant is a loss term in the balance equation, which is given by [27,28]:

$$k_{+,wall} = u_B \frac{A_{eff}}{V}, \tag{5}$$

where $A_{eff} = 2\pi\left(R^2 h_L + RLh_R\right)$ is the area for effective loss, and h_L and h_R are termed the axial and radial coefficients for the positive ion density ratio in the sheath edge with respect to the plasma center, respectively. A simplified form of previously used proportions for low and intermediate densities follow Godyak's formulation [29]:

$$h_L = 0.86\left(3 + \frac{L}{2\lambda_i}\right)^{-0.5}, \tag{6}$$

$$h_R = 0.80\left(4 + \frac{R}{\lambda_i}\right)^{-0.5}. \tag{7}$$

The ion-neutral cross section σ_i needed to calculate the mean free path of the ion λ_i was assumed to be $\sigma_i = 5 \times 10^{-18}$ m^2 [30].

2.1.2. Neutral Recombination and Metastable Extinction on the Chamber Walls

The surface interactions of the neutral particles considered in the model are summarized in Table 1. The coefficient rate for the effective losses of the neutral particles in the wall is given by [31]:

$$k_{n,wall} = \left[\frac{\Lambda_n^2}{D_n} + \frac{2V(2-\gamma)}{Av_g\gamma}\right]^{-1}, \tag{8}$$

where D_n is the diffusion coefficient of neutral particles [31], γ is the recombination/extinction coefficient of neutral particles in the wall, and Λ_n is the effective length of neutral diffusion [31]:

$$\Lambda_n = \left[\left(\frac{\pi}{L}\right)^2 + \left(\frac{2.405}{R}\right)^2 \right]^{-0.5}. \quad (9)$$

2.2. Neutral Gas Power Balance

Collisions between charged and neutral particles lead to significant gas heating. We use the following neutral energy balance equation to calculate the gas temperature (T_g) [32]:

$$\frac{d}{dt}(W_g) = G_{el} + G_{in} - L_p - L_i - L_{in}, \quad (10)$$

where $W_g = \frac{3}{2} n_g k_B T_g$ is the neutral energy density (in J/m^3), $G_{el} = 3\frac{m_e}{M} k_B (T_e - T_g) n_e n_g K_{el}$ is the gas heating due to electron-neutral elastic collisions, $G_{in} = \frac{1}{4} M \overline{v}_i^2 n_e n_g K_{in}$ is the ion-neutral collision heating, $L_p = \kappa \left(\frac{T_g - T_{g0}}{\Lambda_0} \right) \frac{A}{V}$ is the heat flux to the walls. Heat is conducted to the chamber walls by thermal diffusion; the walls are at a fixed temperature T_{g0}. Furthermore, we consider that $L_i = \frac{3}{2} k_B T_g n_e n_g K_{in}$ is the heat loss due to ionization collisions, and $L_{in} = \frac{3}{4} k_B (T_g - T_i) n_e n_g K_{in}$ is the heat loss due to ion-neutral collisions [32,33].

For the expression of G_{el}, $K_{el} \equiv \sigma_{el} \overline{v}_e$ with $\overline{v}_e \equiv (8 k_B T_e / \pi m_e)^{0.5}$ is the electron neutral momentum transfer rate; for G_{in}, $K_{in} \equiv \sigma_i \overline{v}_i$ with $\overline{v}_i \equiv (8 k_B T_i / \pi M)^{0.5}$ is the neutral ion transfer rate (we use $T_i = T_g$); and for L_p, κ is the thermal conductivity of argon gas and $\Lambda_0 = R/2.405 + L/\pi$ is the heat diffusion length [32].

2.3. Electron Power Balance

The global power balance completes the set of differential equations. It can be written as follows [34]:

$$\frac{d}{dt}(W_e) = \frac{(P_{abs} - P_{loss})}{V}, \quad (11)$$

where $W_e = \frac{3}{2} e n_e T_e$ is the energy density of the electron (in J/m^3); P_{abs} is the power absorbed by the plasma; P_{loss} is the lost power; and V is the volume of the discharge chamber. The power loss equation in its most general form is given by [35,36]:

$$P_{loss} = P_{iw} + P_{ew} + P_{ev}, \quad (12)$$

where $P_{iw} = eA\varepsilon_{iw} n_{+s} u_B$ is the power lost by positive ions to the walls, n_{+s} is the ion density in the plasma sheath region, u_B is the Bohm average velocity, and $\varepsilon_{iw} = \frac{T_e}{2} + V_s$ is the average kinetic energy lost by the ions in the walls; here $T_e/2$ is the energy gained by the ion entering the plasma sheath and $V_s = \frac{T_e}{2} ln\left(\frac{M_i}{2\pi m_e}\right)$ is the potential drop in the sheath formed in the reactor walls [37]; $P_{ew} = eA\varepsilon_{ew} n_{es} u_B$ is the power lost by electrons to the chamber walls, where A is the internal area of the chamber, $\varepsilon_{ew} = 2T_e$ is the average kinetic energy per electron lost and n_{es} is the electron density at the sheath edge; and $P_{ev} = e n_e V \sum_X k_{iz} n^{(X)} \varepsilon_c^{(X)}$ is the power lost due to electron–particle reactions.

In the mathematical expression for P_{ev}, the sum is taken over all neutral species x with positive ion counterparts (Ar) with a density $n^{(X)}$, an ionization rate coefficient k_{iz}, and collisional energy loss per electron–ion pair created, $\varepsilon_c^{(X)}$, where the last is [30]:

$$\varepsilon_c^{(X)} = \varepsilon_{iz} + \sum_i \varepsilon_{ex,i}^{(X)} \frac{k_{ex,i}^{(X)}}{k_{iz}} + \frac{3m_e}{M} \frac{k_{el}}{k_{iz}} T_e, \quad (13)$$

where ε_{iz} is the ionization energy of argon; $\varepsilon_{ex,i}^{(X)}$ and $k_{ex,i}^{(X)}$ are the excitation energy and the coefficient rate for the i^{th} excitation process of species X, respectively; k_{el} is the coefficient of the elastic scattering rate of neutral argon; and m_e is the electron mass.

The power absorbed by the plasma, P_{abs}, is given by a direct dependence on the inductive coupling used to excite the plasma. Thus, P_{abs} is the difference between the power delivered by the RF generator by the generator's impedance matcher, P_{RF}, and the power dissipated by the coil (due to ohmic heating), P_{coil} [38]. In this formulation, anomalous field penetration and collision-free heating are not included, so the power delivered to the *RF* is:

$$P_{RF} = \frac{1}{2}(R_{ind} + R_{coil})I_{coil}^2 = P_{abs} + P_{coil}, \tag{14}$$

with P_{abs} and P_{coil} defined as

$$P_{abs} = \frac{1}{2}R_{ind}I_{coil}^2, \tag{15}$$

$$P_{coil} = \frac{1}{2}R_{coil}I_{coil}^2, \tag{16}$$

where R_{ind} and R_{coil} are the effective resistance of the equivalent circuit of the system composed by the plasma and the coil, respectively [12].

In the electrical model, the plasma is generated by means of an electromagnetic field induced by an *RF* current that surrounds the cylindrical chamber of the thruster with a coil of N turns of total length l_c. Since the respective inductance to this coil is given by

$$L_{coil} = \mu_0 \pi \frac{R_c^2 N^2}{l_c}, \tag{17}$$

the coil radius, R_c, is greater than the chamber radius [12,19]. The total impedance of the system is $Z_{ind} = R_{ind} + iL_{ind}\omega$, where R_{ind} and L_{ind} are given by

$$R_{ind} = 2\pi \frac{N^2}{L\omega\varepsilon_0} Re\left[\frac{ikRJ_1(kR)}{\varepsilon_p J_0(kR)}\right], \tag{18}$$

$$L_{ind} = L_{coil}\left(1 - \frac{R^2}{R_c^2}\right) + \frac{2\pi N^2}{L\omega^2\varepsilon_0} Im\left[\frac{ikRJ_1(kR)}{\varepsilon_p J_0(kR)}\right]. \tag{19}$$

So, the respective Bessel functions for zero order and for first order are J_0 and J_1. Since $k = k_0\varepsilon_p^{0.5}$, with $k_0 = \omega/c$ and c is the speed of light, ε_0 is the electrical permittivity in vacuum and the plasma complex permittivity is given by [19]:

$$\varepsilon_p = 1 - \frac{\omega_{pe}^2}{\omega(\omega - i\nu_m)}. \tag{20}$$

2.4. Ar Plasma Chemistry

The chemistry of Ar plasma that was used in this study includes six species: ground state argon (Ar), positive argon ion (Ar^+), metastable argon (Ar^m), resonant argon (Ar^r), atoms in the 4p state (Ar^p), and electrons (e). Ar^m includes the two metastable states $^3P_0$ and $^3P_2$ and Ar^r includes two resonant states $^1P_1$ and $^3P_1$.

The 4p excited state has 10 energy levels in the range of 12.9–13.5 eV. The two metastable levels are combined in the calculations: the radiative and 4p levels. Table 1 lists the reaction set for argon plasma. Collisions between electron and Ar atoms in the excited state (i.e., the R12–R17 reactions in Table 1) were considered as they are believed to play an important role in the particle transfer processes in the argon plasma. The electron impact reaction rate coefficients were calculated by integrating the cross-sections over the assumed Maxwellian distribution.

Table 1. Reactions and their corresponding reaction rates for argon used in the calculations. The subscripts *r* and *m* denote the resonance and metastable levels of the excited state 4*s* and the subscript *p* denotes the excited state 4*p* [21].

N°	Reaction	E_{th}(eV)	Reaction Constant, k (m^3 s^{-1})	Ref.
		Elastic		
1	$Ar + e \rightarrow Ar + e$	-	$k_1 = 2.3 \times 10^{-14} T_e^{1.61} \exp\left(0.06(\ln(T_e))^2 - 0.12(\ln(T_e))^3\right)$	[37]
		Direct ionization		
2	$Ar + e \rightarrow Ar^+ + 2e$	15.76	$k_2 = 2.39 \times 10^{-14} T_e^{0.57} \exp(-17.43/T_e)$	[39]
		Multistep ionization		
3	$Ar^m + e \rightarrow Ar^+ + 2e$	4.43	$k_3 = 2.71 \times 10^{-13} T_e^{0.26} \exp(-4.59/T_e)$	[40]
4	$Ar^r + e \rightarrow Ar^+ + 2e$	3.96	$k_4 = 2.71 \times 10^{-13} T_e^{0.28} \exp(-4.24/T_e)$	[40]
5	$Ar^p + e \rightarrow Ar^+ + 2e$	2.26	$k_5 = 1.09 \times 10^{-12} T_e^{0.29} \exp(-3.42/T_e)$	[31]
		Excitation		
6	$Ar + e \rightarrow Ar^m + e$	11.50	$k_6 = 2.5 \times 10^{-15} T_e^{0.74} \exp(-11.56/T_e)$	[41]
7	$Ar + e \rightarrow Ar^r + e$	11.60	$k_7 = 3.93 \times 10^{-15} T_e^{0.46} \exp(-12.09/T_e)$	[42]
8	$Ar + e \rightarrow Ar^p + e$	12.90	$k_8 = 8.91 \times 10^{-15} T_e^{-0.04} \exp(-14.18/T_e)$	[42]
		De-excitation		
9	$Ar^m + e \rightarrow Ar + e$	−11.50	$k_9 = 2.25 \times 10^{-16} T_e^{-0.17} \exp(-1.65/T_e)$	[41]
10	$Ar^r + e \rightarrow Ar + e$	−11.60	$k_{10} = 6.82 \times 10^{-16} T_e^{0.44} \exp(-0.43/T_e)$	[43]
11	$Ar^p + e \rightarrow Ar + e$	−12.90	$k_{11} = 2.97 \times 10^{-16} T_e^{-0.11} \exp(-1.38/T_e)$	[43]
		Collision between electrons and excited-state Ar atoms		
12	$Ar^m + e \rightarrow Ar^r + e$	1.60	$k_{12} = 3.7 \times 10^{-13}$	[44]
13	$Ar^m + e \rightarrow Ar^p + e$	1.20	$k_{13} = 2.39 \times 10^{-12} T_e^{-0.15} \exp(-1.82/T_e)$	[41]
14	$Ar^r + e \rightarrow Ar^p + e$	1.10	$k_{14} = 2.48 \times 10^{-12} T_e^{-0.16} \exp(-1.79/T_e)$	[41]
15	$Ar^r + e \rightarrow Ar^m + e$	−1.60	$k_{15} = 9.1 \times 10^{-13}$	[45]
16	$Ar^p + e \rightarrow Ar^m + e$	−1.20	$k_{16} = 1.5 \times 10^{-13} T_e^{0.51}$	[46]
17	$Ar^p + e \rightarrow Ar^r + e$	−1.10	$k_{16} = 1.5 \times 10^{-13} T_e^{0.51}$	[46]
		Radiation trapping		
18	$Ar^r \rightarrow Ar + hv$	-	$k_{18} = 1 \times 10^5$ (s^{-1})	[47]
19	$Ar^p \rightarrow Ar^m + hv$	-	$k_{19} = 3 \times 10^7$ (s^{-1})	[48]
20	$Ar^p \rightarrow Ar^r + hv$	-	$k_{20} = 3 \times 10^7$ (s^{-1})	[48]

2.5. Numerical Solution

The global model was solved using the COMSOL Multiphysics 5.4 software. Through the COMSOL differential equation solver, seven of the main variables of the model were calculated, these are the ground state gas density, n_{Ar}; the ionic density, n_{Ar^+}; the metastable density, n_{Arm}; the resonant argon density, n_{Arr}; the density of the atoms in the 4p state, n_{Arp}; the electron temperature, T_e; and the neutral gas temperature, T_g. The calculation is performed by numerically integrating the differential equations of the mass balance and power balance, until the steady-state is reached. The steady-state values of these variables were then used to calculate the quantities of interest for electrical propulsion as detailed in the next topic.

3. Equations and Basic Concepts of Electrical Propulsion

The thrust is the result of the ejection of the propellant in the space and is given by the rate of change of the propellant's momentum over time:

$$T_h = \frac{d(m_p v_{ex})}{dt} = \frac{dm_p}{dt} v_{ex} \quad (21)$$

where m_p is the propellant mass and v_{ex} is the propellant exhaust velocity that does not vary with time. Electric thrusters use sources of electrical energy to create and accelerate charged particles and thus eject them with higher exhaust velocities [8].

The thrust produced by the ion beam through the opening of the transparent grating for the escape of ions is:

$$T_{h_i} = \frac{dm_p}{dt} v_{i_{ex}} = \Gamma_i M A_i v_{bean}, \tag{22}$$

where $v_{i_{ex}} = v_{bean}$ is the exhaust velocity of the ions. The power of the ion beam is given by:

$$P_i = \Gamma_i A_i e V_{grid} = \frac{1}{2} \Gamma_i M A_i {v_{bean}}^2. \tag{23}$$

The thrust of any non-ionized propellant can be estimated from the "random" flow through the grid opening to the neutral atoms, where $v_{g_{ex}} = v_g$ is the exhaust velocity of the neutrals, so [8,19]:

$$T_{h_g} = \frac{dm_p}{dt} v_{g_{ex}} = \Gamma_g M A_g v_g. \tag{24}$$

The power of the neutral flux to the outside of the thruster is given by [12,19]:

$$P_g = \frac{1}{2} \Gamma_g M A_g {v_g}^2. \tag{25}$$

I_{sp} is expressed in units of seconds and can be seen as the ratio between the total thrust, the sum of the neutral thrust and the ion beam thrust, and the propellant consumption rate, which can be expressed as the exhaust velocity divided by gravitational acceleration.

$$I_{sp} = \frac{T_{total}}{\frac{dm_p}{dt} g} = \frac{v_{ex}}{g} \tag{26}$$

The high exhaust velocities or high I_{sp} allow the maximization of the mission's payload mass making electric propulsion attractive. Another advantage of electric propulsion is the ability to vary the I_{sp} throughout a mission, for example by reducing the amount of propellant not converted into charged particles [8].

To study the efficiency from the parameters extracted from the global model, it was decided to analyze the following four efficiencies: (i) the mass utilization efficiency, η_m; (ii) the electrical efficiency, η_e; (iii) the ICP power efficiency, η_{ICP}; and (iv) the total efficiency, η_T, in order to calculate the thrust-to-power ratio, ξ, given in mN/kW, which is used to compare various types of EP as a function of I_{sp}. Starting with the definition of η_m given by the mass flow rate of ions ejected by the mass flow rate of total input in the EP [12,19]:

$$\eta_m = \frac{\Gamma_i A_i}{Q_0} \tag{27}$$

Another way of evaluating the propeller efficiency is from the point of view of η_e, and this is carried out by measuring the power of the jet by the total input power:

$$\eta_e = \frac{P_i + P_g}{P_i + P_g + P_{RF}} \tag{28}$$

The η_{ICP}, unlike the efficiencies η_m and η_e, takes into account the resistive factors:

$$\eta_{ICP} = \frac{R_{ind}}{R_{ind} + R_{coil}} \tag{29}$$

The η_T is the kinetic power produced by the thruster, also known as the jet power, divided by the total power input to the thruster, $P_{input} = \frac{I_b V_b}{\eta_e}$, and is given by:

$$\eta_T = \frac{T^2}{2\dot{m}_p P_{input}} \tag{30}$$

A complementary approach to ion optics can be made by analyzing what happens when particles approach the gratings, resulting in the variation of potential and density in the plasma, in order to meet the equilibrium of the particles or the electrical conditions imposed by the inner walls of the discharge chamber. This region with a very large potential drop compared to the electron temperature is the Child–Langmuir sheath [7,8]. The Child–Langmuir sheath limits extraction to a certain current density. This relationship is expressed by Equation (31) of the Child–Langmuir limit, where J_{CL} is the limit current density, ε_0 is the permittivity in space, and s is the distance between the grids [5].

$$J_{CL} = \frac{4\varepsilon_0}{9}\left(\frac{2q}{M}\right)^{1/2}\frac{{V_{grid}}^{3/2}}{s^2} \tag{31}$$

From Equation (31), the relationship of J_{CL} can be observed, which is directly proportional to the voltage between the grids, V_{grid}, and inversely proportional to the distance between the grids, s. Based on the theory of electrical discharges, Paschen's law describes the behavior of the breakdown voltage (V_b) for the product of the pressure by the distance between the electrodes, according to the V_b values found by Magaldi et al. [49] is possible affirm that for the values of V_{grid} and s multiplied by the pressure inside the thruster, there is no possibility of a dielectric breakdown between the grids in the configuration used in this study.

To form a plasma sheath to accelerate the high-energy ions and reflect the electrons, the limiting distance of the plasma must be around the Child–Langmuir length. Therefore, the ideal distance, s, between the grids for a better extraction, the Child–Langmuir length, is proportional to the mass of the ions [25].

4. Results and Discussion

As previously highlighted, this global model study was carried out in two different scenarios: (1) one considering the metastable species Ar^r and Ar^p and (2) the other without considering these species. Thus, the comparison of the results with the complete set and another reduced set of reactions allowed for a better understanding of the real influence of metastable species in the proposed global model and how this accounting affected the GIT efficiencies.

Figure 2 presents the current density through the grids for the two reaction set configurations as a function of RF power. In this figure, it is evidenced how the ion current density without the two excited species is higher than with the metastables, this can be explained by the fact that the absence of the complete set is compensated for in the densities of the other species as shown in Figure 3.

From Equation (32), the Child–Langmuir limit is plotted for both cases, and the two dashed lines are at 121.48 A/m^2 and 273.33 A/m^2. Two dashed vertical lines represent the corresponding power of 427.5 W for the complete set (case 1) and 848.2 W for the incomplete set (case 2). Figure 3 shows the densities of each species (Ar, Ar^+, Ar^m, Ar^r, Ar^p, and e^-) calculated by the global model based on the parameters of Table 2, based on the settings used in the references [12,19]. The RF power range chosen between 178 W and 1600 W corresponds to a current of 2 A to 10 A in the ICP coil, as a thruster of similar in size to the one modeled in this study is normally greater than 200 W [12].

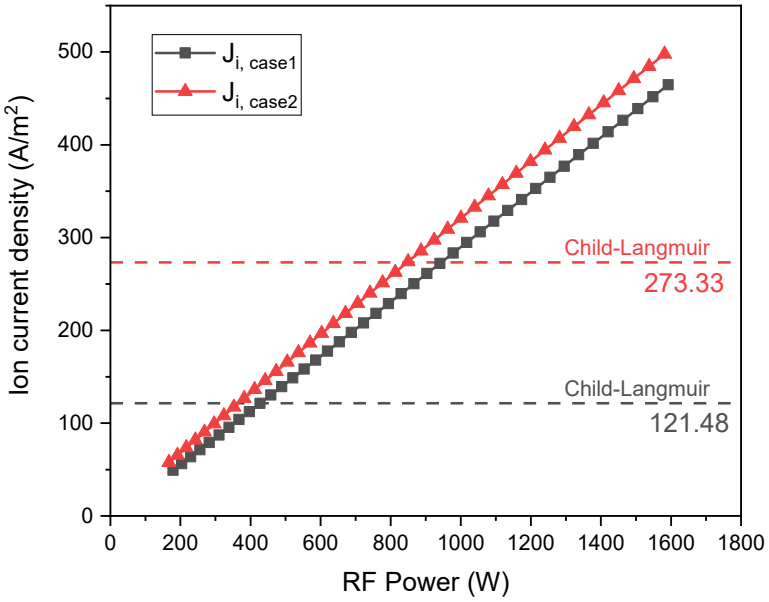

Figure 2. Current density through the grids for the two reaction set configurations as a function of RF power. The dashed lines indicate the Child–Langmuir limit for the respective inlet currents, and at a pressure of 2 mTorr.

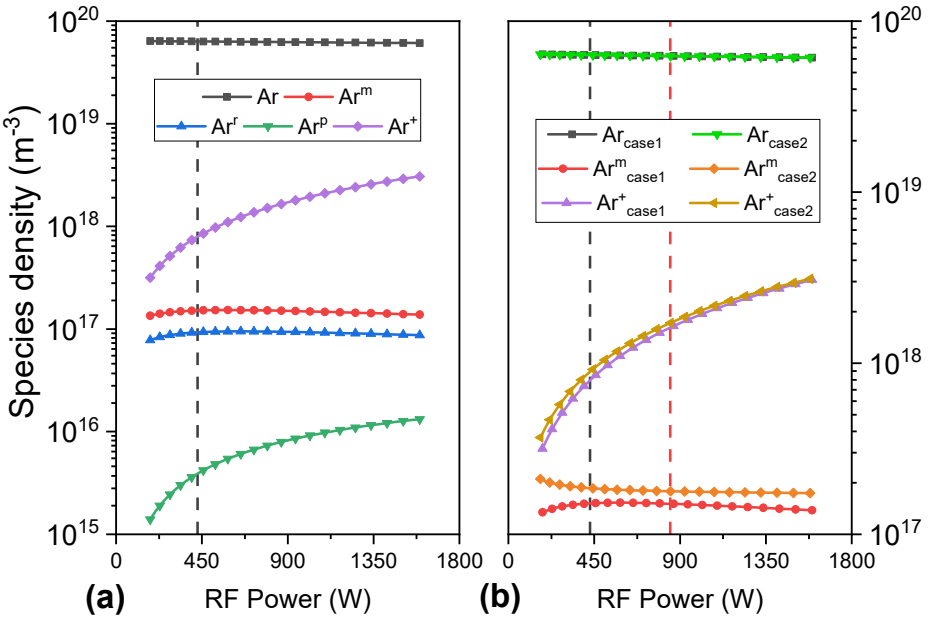

Figure 3. Graphs of the densities of neutral, excited, and charged species in the thruster chamber as a function of RF power. (**a**) Species densities for the complete set of reactions. (**b**) Comparison of common species for the cases 1 and 2. Pressure = 2 mTorr.

Table 2. This table shows the argon constants and other parameters used in the global model.

Dimensions	Gas Injection	Grid Settings	Coil Properties	Argon Constants
R = 6 cm L = 10 cm R_c = 7 cm	$Q_0 = 4.5 \times 10^{18}$ s^{-1} Q_{sccm} = 10 sccm	$\beta_i = 0.7$ $\beta_g = 0.3$ s = 1.5 mm V_{grid} = 1000 V	N = 5 turns $L_{coil} = 4.84 \times 10^{-6}$ H R_{coil} = 2 Ω	M = 40 uma $\kappa = 0.0181$ Wm^{-1} K^{-1} $\sigma_i = 10^{-18}$ m^2

Still in Figure 3, it is possible to observe a subtle drop in the neutral argon density, which may be associated with a gradual drop in neutral atoms as a consequence of excitations to metastable states and ionization. A second reason that explains this fact is the

increase in the temperature of the gas, T_g, with the increase of the RF power, as shown in Figure 4. There is an increase in the thermal velocity of the atoms leaving the propellant, reducing the density of neutral atoms. In the ionized argon curve, the degree of ionization shows a small, almost constant and proportional increase over the entire power range. With the percentages close to 3.5% and 4.2% when entering the Child–Langmuir limit range.

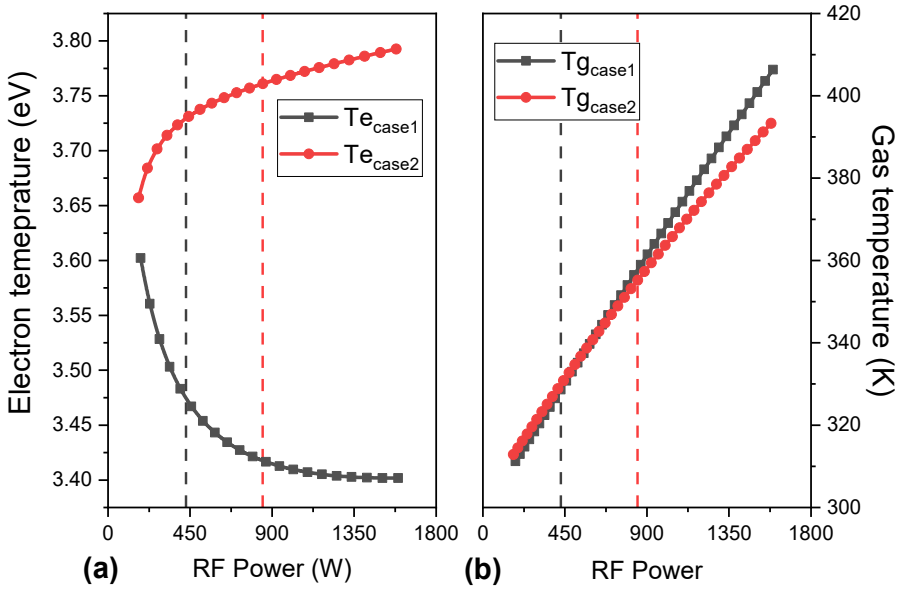

Figure 4. Electron temperature (**a**) and neutral gas temperature (**b**) as a function of RF power for the cases 1 and 2. Pressure = 2 mTorr.

Argon plasma has a higher density of excited species than other more commonly used propellants, such as xenon and reference iodine [12,19]. These energy levels require less energy for ionization, favoring the replacement of argon ions over the plasma volume. In addition to presenting a higher density of neutral and ionized species compared to the aforementioned xenon and iodine, as a result of their smaller size. This higher ion density added to the almost immediate replacement of ions through the excited species allows for a possible compensation with respect to their lower atomic mass and higher ionization energy.

It is interesting to note in Figure 4 that the T_e for the complete set decreases as the power is increased, which shows that this growth rate of the ionization curve is caused by the interactions of electrons with metastable species, which have a lower energy potential to ionize and thus the ionization equilibrium is maintained quickly without requiring a higher T_e, as in the beginning of plasma generation with energetically charged species. On the other hand, the T_e with the incomplete set does not have this energy compensation provided by the metastables, causing the need for a higher T_e so that the electrons can ionize the neutral argon atoms. The T_e drop of the complete set is significant, of almost 0.2 eV, with the subsequent increase in power reaching 3.4 eV at the Child–Langmuir limit. This favors the hypothesis that after ionic equilibrium is established, the energy exchange from collisions with electrons occurs with a lower T_e. This small temperature difference of T_g with the complete set and without the complete set is due to the account of the greater number of interactions between the neutral species in the multistep process of argon ionization.

For a better understanding of which gain and loss terms in Equation (10) contribute more to the heating of the gas as the power is increased, these were evaluated separately as a function of the RF power and are shown in Figure 5. The Equation (10) is based on the study developed by Chabert et al. and Grondein et al. [12,19]. Only gas-heating gains due to electron-neutral elastic collisions, G_{el}, and from ion-neutral collision heating, G_{in}, were accounted for, while the only losses are accounted for by heat flow to the walls, L_p.

Other collisional losses were accounted for but do not enter the overall neutral gas energy balance. These collisional losses added to the equilibrium equation were called the heat loss due to ionization collisions, L_i, and the heat loss due to ion-neutral collisions, L_{in}. It is undeniable that the high energy loss of L_{in} ended up being counted as an energy gain species in this case, but it was preferred to keep it as a loss term, as defined by Golant et al. in [33] and highlighted by Liard et al. in [32]. This thermal gain caused by not accounting for L_{in} is reflected in an increase in T_g. In terms of T_g, it is not a value that can interfere in the calculation of species densities nor in their values along the RF power.

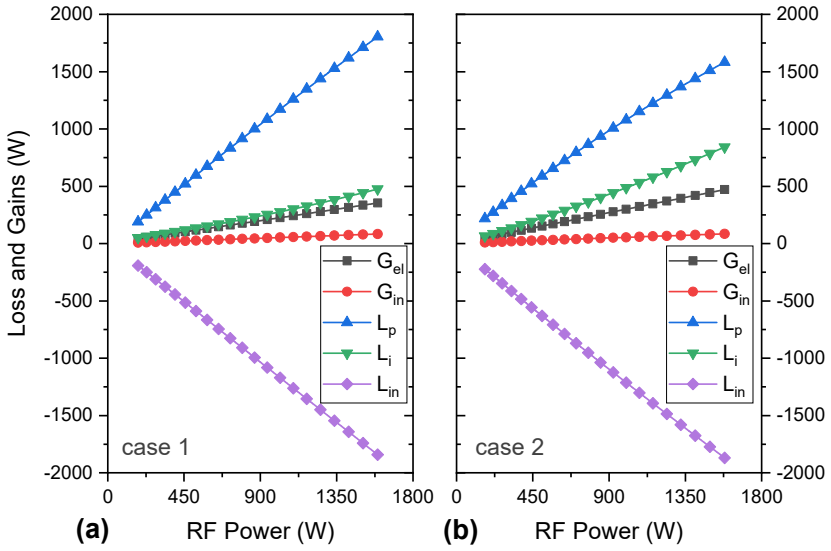

Figure 5. Comparison of the contributions of the gain and loss terms of the differential equation of neutral energy balance of the gas presented in Equation (10) for both cases: with (**a**) and without (**b**) Ar^r and Ar^p species, as a function of the RF power. Pressure = 2 mTorr.

It is understandable to raise the question regarding the ability of these ion-neutral collisions plus the metastable species from the complete set to result in an increase in the temperature T_g. In the global model, it is not common to delve deeper into the study of possible inaccuracies that the adopted assumptions may cause, but in general evaluations, the energy balances are associated within the system of differential equations and in this way this energy from L_{in} does not go to the T_g and goes somewhere else, which could be the electrons. However, the conjecture presented—that the electrons, when receiving this energy, would raise the T_e—was not proven when studying the contribution of this energy loss, since the T_e and the density of the species did not show variation. The maintenance of densities brings the information that this energy was not enough to form new ionized species and that because the plasma is semi-neutral, it would justify an increase in the density of electrons in an amount similar to that of positive charges, which in turn could alter until. As a result of the subsequent results, the unaccounted energy may be linked to the kinetic energy of the species, which would result in an increase in T_g.

Figure 6 shows the contribution to ionization as the RF power is increased. It is important to remember that when talking about the incomplete set, it still presents the Ar^m species and that is why the multistep is discussed in this case. In Figure 6 it is evident with increasing RF power that the Ar^r and Ar^p species greatly increase the contribution to ionization, this fact being confirmed by all the other analyzes presented so far. The energy that the electron spends on average to perform an ionization is provided by collision energy. The collisional energy is a function of the reaction constants; therefore, even if the excited species were disregarded in the calculation and considering the balance of particles in addition to ionizations and elastic collisions, the electron would have spent energy in the production of metastables [17]. In case the excited species were not accounted for, a smaller number of excitations were performed, which resulted in a reduction of the energy spent

for the generation of an electron–ion pair. The increase in L_i shown in Figure 5, means that the probability of ionization tends to increase as the power increases, and this may be motivated by a smaller number of reactions of other types. The reactions, similar to those of the excited species, are a direct consequence of the ionization constants rising in front of the other distributions. Therefore, the population of high-energy electrons produces ionizing reactions, thus decreasing T_e, as shown in Figure 4.

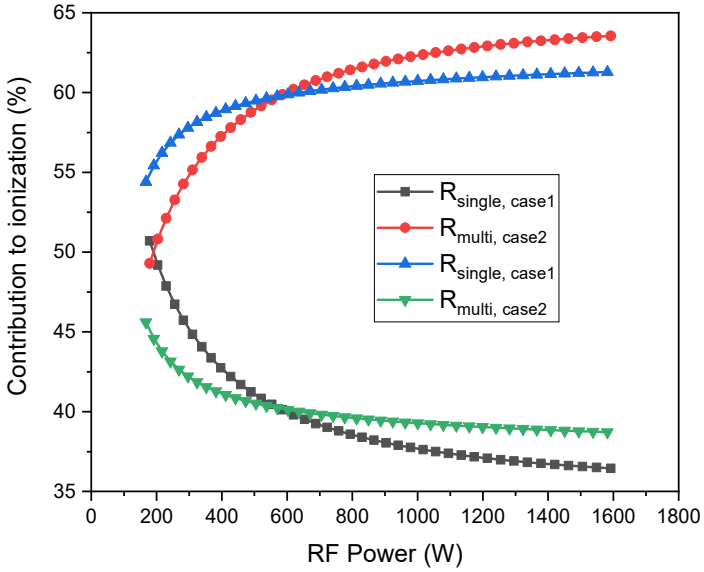

Figure 6. Comparison between contributions to ionization for cases with (case 1) and without (case 2) the complete set of reactions as a function of RF power. Pressure = 2 mTorr.

Figure 7 shows a comparison between the inductively coupled plasma (ICP) power transfer efficiency, η_{ICP}; the mass transfer efficiency, η_m; the electrical transfer efficiency, η_e; and the total efficiency, η_T, for both models with and without the complete set. In terms of the comparison between with and without the complete set, it is evident that the η_{ICP} does not change; the η_e and η_m for the complete set tend to be smaller, but with a small increase for η_e and a constant increase that is slightly smaller than that without η_m when it is raised to RF power; and finally, the η_T which presents a reasonable drop. These drops present a characteristic that is much closer to real efficiency, and although they are a reduction in efficiency, they do not represent a negative point, since they are very positive results.

The electrical efficiency remained close to 80% (a very good value for argon, which has a high ionization potential), which confirms that the energy transfer through the excited species is a great potential of the argon propellant. The low mass transfer efficiency was expected, due to the size of the argon atom and its molar mass. Total efficiency is a parameter that has appeared more frequently in the new literature and serves as a reference between the different types of thrusters and their different physical properties.

Now taking what has been shown in Figure 6, where it is evident that step-wise ionization favors an increase in the global ionization as the contribution of the Ar^r and Ar^p species reduces the energy consumption in the formation of ions. However, the contribution in case 1 of low RF power is smaller than in case 2. This reflects a reduction in the aforementioned efficiencies but does not reflect a loss of efficiency, rather an efficiency closer to what was expected for reality. In this way, the comparison of the thrust produced with the accounting of energetic species, as well as some efficiencies, was lower, as shown in Figure 8. For an RF power of 450 W, approximately 40 mN was delivered, which represents a remarkable thrust value for electric thrusters.

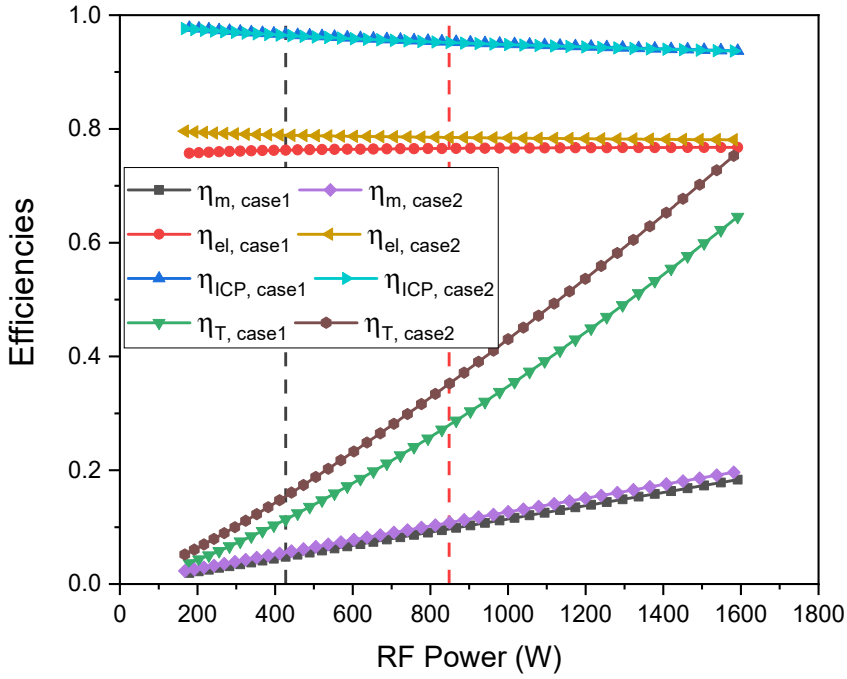

Figure 7. Mass transfer efficiency, η_m; ICP power transfer efficiency, η_{ICP}; electrical efficiency, ηe; and total efficiency, η_T, calculated by global model with (case 1) and without (case 2) the complete set of reactions as a function of the RF Power. Pressure = 2 mTorr.

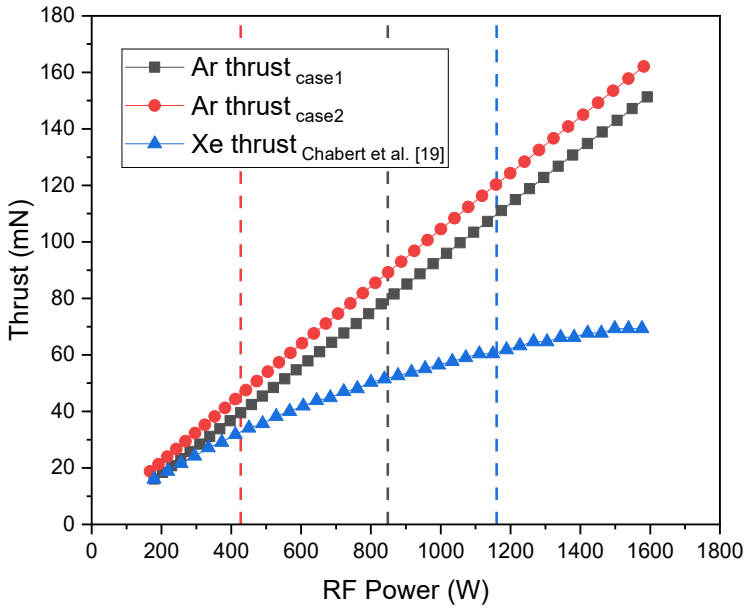

Figure 8. Comparison of the thrust produced by Ar ions calculated by global model with (case 1) and without (case 2) the complete set of reactions as a function of RF Power. The data in blue were adapted from Chabert et al. [19] and are relative to global model of xenon plasma thruster. Pressure = 2 mTorr.

With the intention of obtaining a comparison, knowing that in the literature no results were found with the desired experimental parameters, an alternative was to compare the results of Chabert et al., where the thruster was calculated by the global model of xenon plasma [19]. This comparison must be seen based on the Child–Langmuir limits, which physically delineate where the result found by the simulation is possible. The Child–Langmuir limits of Figure 8 are: 428 W for argon (case 2), 848 W for argon (case 1), and 1160 W for xenon [19], corresponding to approximately 45 mN, 80 mN, and 60 mN, respectively. Although in Figure 8, for high power values, the thrust produced by argon exceeds

that produced by xenon, the Child–Langmuir limit of argon was exceeded, therefore not corresponding to reality. Generally speaking, for RF power up to 430 W the thrusts for both plasmas are close.

5. Conclusions

In this work, a global model was developed to study electric propulsion with two extraction grids operating with argon gas at a pressure of 2 mTorr. The analysis of the generated plasma was divided into scenarios with (multi-step ionization or case 1) and without (single-step ionization or case 2) the complete reaction set, having explored a set of 20 reactions in the plasma volume. Additionally, the model includes the energy balance of the neutral species, thus allowing the determination of the neutral gas temperature and thus verifying the propellant heating level for the investigated operational parameters.

It was expected that the metastable state Ar^m would make a significant contribution to the mechanism of maintaining the ion density in the creation and extraction process of the thruster due to its long lifetime, in the order of a few seconds. The novelty was being able to make this comparison of the other resonant species, Ar^r, and the ten energy levels of argon corresponding to the 4p configuration, Ar^p, in a global model made in detail for a GIT.

There was also a strong dependence of the density of ions and excited species with the power, which increases by up to an order of magnitude for the investigated power range. On the other hand, the electron temperature was reduced with RF power, corroborating with the results observed in the literature.

In the propulsion aspects, a thrust of practically 40 mN at 450 W with the complete set was observed, the efficiencies found were used as a comparison with other types of electric propulsion, being able to satisfy a group of specific missions that require up to 3000 s of specific impulse and other parameters used.

Author Contributions: Conceptualization, B.M., R.P. and A.d.S.S.; methodology, J.K. and B.M.; software, B.M. and R.P.; writing—original draft preparation, B.M., J.K. and R.P.; writing—review and editing, B.M., J.K., R.P. and A.d.S.S.; supervision, R.P. and A.d.S.S.; funding acquisition, R.P. and A.d.S.S. All authors have read and agreed to the published version of the manuscript.

Funding: This research received no external funding.

Institutional Review Board Statement: Not applicable.

Informed Consent Statement: Not applicable.

Data Availability Statement: Not applicable.

Acknowledgments: B.M. and J.K. thank the Coordenação de Aperfeiçoamento de Pessoal de Nível Superior—CAPES for master and doctoral grants, respectively (Finance Code 001).

Conflicts of Interest: The authors declare no conflict of interest.

References

1. Barrutia, J.M.; Echebarria, C. Effect of the COVID-19 pandemic on public managers' attitudes toward digital transformation. *Technol. Soc.* **2021**, *67*, 101776. [CrossRef] [PubMed]
2. Levchenko, I.; Xu, S.; Mazouffre, S.; Lev, D.; Pedrini, D.; Goebel, D.; Garrigues, L.; Taccogna, F.; Bazaka, K. Perspectives, frontiers, and new horizons for plasma-based space electric propulsion. *Phys. Plasmas* **2020**, *27*, 02060. [CrossRef]
3. Rakhimov, R.G.; Kharlan, Y.Y.; Uzhinsky, I. Numerical simulation of plasma discharge in RF ion thruster. In Proceedings of the 36th International Electric Propulsion Conference, Vienna, Austria, 15–20 September 2019.
4. Conde, L.; Domenech-Garret, J.L.; Donoso, J.M.; Damba, J.; Tierno, S.P.; Alamillo-Gamboa, E.; Castillo, M.A. Supersonic plasma beams with controlled speed generated by the alternative low power hybrid ion engine (ALPHIE) for space propulsion. *Phys. Plasmas* **2017**, *24*, 123514. [CrossRef]
5. Goebel, D.M.; Katz, I. *Fundamentals of Electric Propulsion: Ion and Hall Thrusters*; John Wiley & Sons: Hoboken, NJ, USA, 2008.
6. Mazouffre, S. Electric propulsion for satellites and spacecraft: Established technologies and novel approaches. *Plasma Sources Sci. Technol.* **2016**, *25*, 033002. [CrossRef]

7. Jahn, R.G.; Choueiri, Y. *Electric Propulsion Encyclopedia of Physical Science and Technology 5*, 3rd ed.; Academic: San Diego, CA, USA, 2002.
8. Charles, C. Plasmas for spacecraft propulsion. *J. Phys. D Appl. Phys.* **2019**, *42*, 163001. [CrossRef]
9. Garrigues, L.; Coche, P. Electric propulsion: Comparison between different concepts. *Plasma Phys. Control. Fusion* **2011**, *53*, 124011. [CrossRef]
10. Ahedo, E. Plasmas for space propulsion Plasma. *Phys. Control. Fusion* **2011**, *53*, 124037. [CrossRef]
11. Sutton, G.P.; Biblarz, O. *Rocket Propulsion Elements*; Wiley: New York, NY, USA, 2017.
12. Grondein, P.; Lafleur, T.; Chabert, P.; Aanesland, A. Global model of an iodine gridded plasma thruster. *Phys. Plasmas* **2016**, *23*, 033514. [CrossRef]
13. Williams, L.T.; Walker, M.L.R. Ion production cost of a gridded helicon ion thruster. *Plasma Sources Sci. Technol.* **2013**, *22*, 055019. [CrossRef]
14. Ichihara, D.; Matsuba, T.; Iwakawa, A.; Sasoh, A. High-Specific-Impulse Electrostatic Thruster with Argon Propellant. *J. Propuls. Power* **2020**, *36*, 256–263. [CrossRef]
15. Williams, L.T.; Walker, M.L.R. Initial Performance Evaluation of a Gridded Radio Frequency Ion Thruster. *J. Propuls. Power* **2014**, *30*, 645–655. [CrossRef]
16. Yamasaki, J.; Yokota, S.; Shimamura, K. Performance enhancement of an argon-based propellant in a Hall thruster. *Vacuum* **2019**, *167*, 520–523. [CrossRef]
17. Karnopp, J.; Magaldi, B.; Sagás, J.; Pessoa, R. The effect of excited species on the collisional energy of argon inductively coupled plasmas: A global model study. *Plasma* **2022**, *5*, 30–43. [CrossRef]
18. Alves, L.L.; Bogaerts, A.; Guerra, V.; Turner, M.M. Foundations of modelling of nonequilibrium low-temperature plasmas. *Plasma Sources Sci. Technol.* **2018**, *27*, 023002. [CrossRef]
19. Chabert, P.; Monreal, J.A.; Bredin, J.; Popelier, L.; Aanesland, A. Global model of a gridded-ion thruster powered by a radiofrequency inductive coil. *Phys. Plasmas* **2012**, *19*, 073512. [CrossRef]
20. Dietz, P.; Becker, F.; Keil, K.; Holste, K.; Klar, P.J. Performance of a rf neutralizer operating with noble gases and iodine. *Eur. Phys. J. Appl. Phys.* **2020**, *91*, 10901. [CrossRef]
21. Pessoa, R.S.; Sismanoglu, B.N.; Gomes, M.P.; Medeiros, H.S.; Sagás, J.C.; Roberto, M.; Maciel, H.S.; Petraconi, G. Chemistry Studies of Low Pressure Argon Discharges: Experiments and Simulation. In *Argon: Production, Characteristics and Applications*; Bogos, N.S., Maciel, H.S., Radmilovic-Radjenovic, M., Pessoa, R.S., Eds.; Nova Science Publishers, Inc.: Hauppauge, NY, USA, 2013.
22. Radd, H. A Survey of Spatial Problems. *J. Am. Rocket. Soc.* **1945**, *62*, 28–29. [CrossRef]
23. Volkmar, C.; Ricklefs, U. Implementation and verification of a hybrid performance and impedance model of gridded radio-frequency ion thrusters. *Eur. Phys. J. D* **2015**, *69*, 227. [CrossRef]
24. Volkmar, C. Selbstkonsistente Numerische 1D/3D Hybridmodellierung von Radiofrequenz-Ionentriebwerken. Ph.D. Thesis, Justus Liebig University Giessen, Giessen, Germany, 23 July 2015.
25. Magaldi, B.V.; Pessoa, R.S.; Da Silva Sobrinho, A.S. A global model study of argon plasma chemistry used as propellant of a gridded ion thruster. *Rev. Bras. Appl. Vácuo* **2021**, *40*, e0121. [CrossRef]
26. Monahan, D.D.; Turner, M.M. Global models of electronegative discharges: Critical evaluation and practical recommendations. *Plasma Sources Sci. Technol.* **2008**, *17*, 045003. [CrossRef]
27. Kim, S. An Improved Global Model for Electronegative Discharge and Ignition Conditions for Peripheral Plasma Connected to a Capacitive Discharge. Ph.D. Thesis, University of California, Berkeley, CA, USA, 2006.
28. Raimbault, J.-L.; Chabert, P. Edge-to-center plasma density ratio in high density plasma sources. *Plasma Sources Sci. Technol.* **2009**, *18*, 014017. [CrossRef]
29. Godyak, V.A. *Soviet Radio Frequency Discharge Research*; Delphic Associates, Inc.: Falls Church, VA, USA, 1986.
30. Lieberman, M.A.; Gottscho, R.A. Design of High-Density Plasma Sources for Materials Processing. In *Physics of Thin Films*; Francombe, M., Vossen, J., Eds.; Academic: New York, NY, USA, 1994; Volume 18.
31. Thorsteinsson, E.G.; Gudmundsson, J.T. A global (volume averaged) model of a Cl_2/Ar discharge: I. Continuous power. *J. Phys. D Appl. Phys.* **2010**, *43*, 115201. [CrossRef]
32. Liard, L.; Raimbault, J.-L.; Rax, J.-M.; Chabert, P. Plasma transport under neutral gas depletion conditions. *J. Phys. D Appl. Phys.* **2007**, *40*, 5192–5195. [CrossRef]
33. Golant, V.; Zhilinsky, A.P.; Sakharov, I.E.; Brown, S.C. *Fundamentals of Plasma Physics*; Wiley: New York, NY, USA, 1980.
34. Toneli, D.A.; Pessoa, R.S.; Roberto, M.; Gudmundsson, J.T. On the formation and annihilation of the singlet molecular metastables in an oxygen discharge. *J. Phys. D Appl. Phys.* **2015**, *48*, 325202. [CrossRef]
35. Lee, C.; Lieberman, M.A. Global model of Ar, O_2, Cl_2, and Ar/O_2 high density plasma discharges. *J. Vac. Sci. Technol. A* **1994**, *13*, 368. [CrossRef]
36. Toneli, D.A.; Pessoa, R.S.; Roberto, M.; Gudmundsson, J.T. A global model study of low pressure high density CF_4 discharge. *Plasma Sources Sci. Technol.* **2019**, *28*, 025007. [CrossRef]
37. Lieberman, M.A.; Lichtenberg, A.J. *Principles of Plasma Discharges and Materials Processing*, 2nd ed.; Wiley: New York, NY, USA, 2005.
38. Chabert, P.; Braithwaite, N. *Radio-Frequency Plasmas*; Cambridge University Press: Cambridge, UK, 2011.

39. Straub, H.C.; Renault, P.; Lindsay, B.G.; Smith, K.A.; Stebbings, R.F. Absolute partial and total cross sections for electron-impact ionization of argon from threshold to 1000 eV. *Phys. Rev. A* **1995**, *52*, 1115. [CrossRef]
40. Ali, M.A.; Stone, P. Electron impact ionization of metastable rare gases: He, Ne and Ar. *J. Mass Spectrom.* **2008**, *271*, 51. [CrossRef]
41. Mityureva, A.A.; Smirnov, V.V. Electronic Excitation of Ar Atoms to Metastable States and from Metastable to Higher States. *Opt. Spectrosc.* **2004**, *97*, 508. [CrossRef]
42. Deutsch, H.; Becker, K.; Grum-Grzhimailo, A.N.; Bartschat, K.; Summers, H.; Probst, M.; Matt-Leubner, S.; Mark, T.D. Calculated cross sections for the electron-impact ionization of excited argon atoms using the DM formalism. *J. Mass Spectrom.* **2004**, *233*, 39.
43. Hayashi, M. *A Set of Electron-Ar Cross Sections with 25 Excited States*; National Institution for Fusion Science: Tokyo, Japan, 2003.
44. Ferreira, C.M.; Loureiro, J.; Richard, A. Populations in the metastable and the resonance levels of argon and stepwise ionization effects in a low-pressure argon positive column. *J. Appl. Phys.* **1985**, *57*, 82. [CrossRef]
45. Gudmundsson, J.T.; Thorsteinsson, E.G. Oxygen discharges diluted with argon: Dissociation processes. *Plasma Sources Sci. Technol.* **2007**, *16*, 399. [CrossRef]
46. Ashida, S.; Lee, C.; Lieberman, M.A. Spatially averaged (global) model of time modulated high density argon plasmas. *J. Vac. Sci. Technol. A* **1995**, *13*, 2498. [CrossRef]
47. Hurst, G.S.; Wagner, E.B.; Payne, M.G. Energy transfer from argon resonance states to nitrogen, hydrogen, and nitric oxide. *J. Chem. Phys.* **1974**, *61*, 3680. [CrossRef]
48. Lee, M.-H.; Jang, S.-H.; And Chung, C.-W. On the multistep ionizations in an argon inductively coupled plasma. *Phys. Plasmas* **2006**, *13*, 053502. [CrossRef]
49. Magaldi, B.V.; Pessoa, R.S.; Cesare, M.P.; Ribeiro, A.A.; Martins, C.A.; da Silva Sobrinho, A.S. Control and Data Acquisition System to Study Dielectric Breakdown in Low-Pressure Dc Plasma Reactor with Parallels Electrodes. *Rev. Bras. Appl. Vac.* **2021**, *40*, E1821. [CrossRef]